Maximal Potential Energy Transport: A Variational Principle for Solidification Problems

A. J. Wells,[1,4] J. S. Wettlaufer,[1,2,4] and S. A. Orszag[3,4]

[1]*Department of Geology and Geophysics, Yale University, New Haven, Connecticut 06520, USA*
[2]*Department of Physics, Yale University, New Haven, Connecticut 06520-8109, USA*
[3]*Department of Mathematics, Yale University, New Haven, Connecticut 06520-8283, USA*
[4]*Program in Applied Mathematics, Yale University, New Haven, Connecticut 06520, USA*

(Received 15 March 2010; revised manuscript received 19 November 2010; published 13 December 2010)

We analyze numerically the mechanisms controlling the spacing of chimneys—channels devoid of solid—in two-dimensional mushy layers formed by solidifying a binary alloy. Chimneys are the principal conduits through which buoyancy effects material transport out of the mushy layer and into the liquid from which it formed. Experiments show a coarsening of chimney spacing; we pursue the hypothesis that the spacing adjusts to optimize material transport and hence maximize the rate of removal of potential energy stored in the mushy layer. The optimal solute flux increases approximately linearly with the mush Rayleigh number. However, for spacings below a critical value, the chimneys collapse and solute fluxes cease, revealing a hysteresis between chimney convection and no flow. The results are consistent with a variational principle controlling the dynamics of this dissipative system.

DOI: 10.1103/PhysRevLett.105.254502 PACS numbers: 47.20.Bp, 05.70.Ln, 47.20.Hw, 47.54.−r

Variational principles are a cornerstone of physics with the trajectory of a system determined by the extremum of the action. A common example is an action defined as the time integral of the Lagrangian. However, variational principles for nonlinear dissipative systems constitute a topic of long-standing debate because the nonconservation of phase space volume implies that such systems are not Hamiltonian [1]. Successful examples include shear-driven turbulence [2] and turbulent Rayleigh-Bénard convection, where bounds on the heat flux compare favorably with scaling arguments [3]. In this Letter, we demonstrate that a variational principle underlies convection in a *mushy layer*: a reactive porous medium formed during solidification of a binary alloy [4]. In addition to shedding light on the dynamics of nonlinear dissipative systems, this problem has direct applications in many natural and industrial settings. For example, such convection governs brine drainage from young sea ice and the consequent buoyancy forcing of the polar oceans [5].

Under common growth conditions, morphological instability of the solid-liquid interface generates a mushy layer: a reactive porous medium of solid dendrites bathed in concentrated fluid. The interstitial fluid can become convectively unstable, resulting in buoyancy-driven convection within the mushy layer [4]. Convection drives the flow of fluid depleted (enriched) in solute into regions of high (low) solute concentration, causing local dissolution (growth) of the solid matrix because the interstitial fluid adjusts to maintain local thermodynamic equilibrium. Regions of low solid fraction have high permeability, and hence flow focusing accelerates the growth of the instability. The nonlinear growth of this instability leads to channels devoid of solid, or *chimneys*, which are the principal conduits for drainage of solute from the layer. Experiments show that, for a constant solidification rate, the chimneys are regularly spaced (e.g., [6]), whereas during transient growth the mean spacing increases over time as the mushy layer thickens [5,7].

The onset of convection and local dissolution is predicted by linear and weakly nonlinear stability analyses (see Ref. [4]), but after chimneys form a different approach is needed to account for the combination of porous flow in the mushy region and pure liquid flow in the chimney. Previous analyses treated either an isolated chimney [8] or modeled dynamics that arise with a periodic array of chimneys of imposed spacing [9,10]. These require the areal number density of chimneys to be specified *a priori*; any subsequent prediction of solute fluxes relies on an independent theoretical prediction of the spacing of chimneys.

We hypothesize that the chimney spacing l adjusts to maximize drainage of potential energy from the mushy layer, and thus the dissipative dynamics are governed by a variational principle yielding optimal solute fluxes. The resulting properties are determined numerically for two-dimensional steady-state solidification and used to reconcile behavior observed during transient growth. Figure 1 describes the two-component mixture of liquid concentration C and temperature T that is translated at a velocity V between hot and cold heat baths. Solidification depletes the liquid of solute, reducing the density to drive convection; we calculate the solute flux with a periodic array of chimneys.

The so-called ''ideal'' mushy layer theory describes conservation of heat and solute, along with incompressible Darcy flow. We draw upon an analysis of boundary conditions and their implications developed previously [9–12] together with a fully time-dependent treatment to reveal

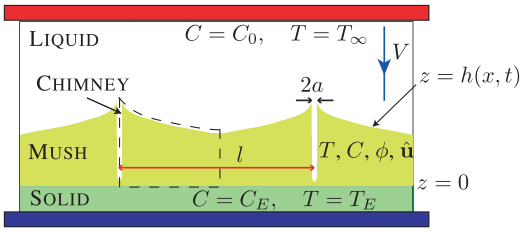

FIG. 1 (color online). A two-dimensional mushy layer formed between two heat baths pulled at velocity V aligned with the gravitational acceleration $g\mathbf{k}$. The overlying liquid has constant far-field temperature T_∞ and concentration C_0, and the mush solidifies at eutectic temperature T_E and concentration C_E at $z = 0$. For a periodic array of chimneys, of dimensional width $2\hat{a}(z, t)$ and imposed spacing l, we exploit symmetry to solve for the properties of a mushy layer of thickness $h(x, t)$ within the dashed outline. The specific heat capacity c_p and thermal diffusivity κ are assumed constant across solid and liquid phases, and the fluid has dynamic viscosity μ and density $\rho_0 g\beta(C - C_E)$ for constant solutal coefficient β and reference density ρ_0. This describes aqueous NH_4Cl solidified from below, among other systems.

the hypothesized variational principle. Within the mushy layer, T and C are coupled by local thermodynamic equilibrium and hence lie on the liquidus curve $T = T_L(C) = T_E + \Gamma(C - C_E)$, where Γ is constant, so that the local dimensionless temperature is $\theta = [T - T_L(C_0)]/\Gamma\Delta C = (C - C_0)/\Delta C$, where C_0 is the bulk liquid concentration and $\Delta C = C_0 - C_E$. Then θ and solid fraction ϕ are solved for, and we calculate the Darcy velocity $\mathbf{u} = (\psi_x, -\psi_z)$ by generating a vorticity equation for the dimensionless stream function ψ, assuming that the fluid density depends linearly on concentration and that the mushy layer has permeability $\Pi = \Pi_0(1 - \phi)^3$. Velocities, lengths, and times are scaled by V, $l_T = \kappa/V$, and κ/V^2, respectively, from which we obtain six dimensionless parameters governing the system:

$$R_m = \frac{\rho_0 g\beta\Delta C\Pi_0 l_T}{\mu\kappa}, \quad \mathcal{C} = \frac{C_S - C_0}{\Delta C}, \quad \mathrm{Da} = \frac{\Pi_0 V^2}{\kappa^2},$$
$$\theta_\infty = \frac{T_\infty - T_L(C_0)}{\Gamma\Delta C}, \quad \mathcal{S} = \frac{L}{c_p\Gamma\Delta C}, \quad \lambda = \frac{Vl}{2\kappa}. \tag{1}$$

The mushy layer Rayleigh number R_m describes the ratio of buoyancy to dissipation, and the Darcy number Da characterizes the mushy layer permeability. The Stefan number $\mathcal{S}$, concentration ratio $\mathcal{C}$, and scaled temperature θ_∞ characterize the imposed thermodynamic conditions.

Rather than solving directly for the overlying fluid layer, we apply a boundary layer approximation to describe its influence on the mushy layer. We assume constant pressure at the mush-liquid interface [11] and that in the absence of solutal diffusion the fluid region has uniform concentration C_0 away from plumes exiting the mushy layer [9]. The position of the mush-liquid interface is determined by the condition of marginal equilibrium $\theta = 0$ at $z = h$, and hence continuity of salinity and normal heat fluxes give $\phi = 0$ and $\mathbf{n} \cdot \nabla T|_-^+ = 0$ at $z = h$. Applying a boundary layer approximation that balances advection and diffusion of heat across isotherms of curvature $\nabla \cdot \mathbf{n}$ yields

$$\mathbf{n} \cdot \nabla\theta = \theta_\infty[\nabla \cdot \mathbf{n} - (\mathbf{u} - \mathbf{k}) \cdot \mathbf{n}]. \tag{2}$$

The lower boundary $z = 0$ is impermeable and fixed at the eutectic temperature ($\theta = -1$), and we apply symmetry conditions at the right-hand boundary of the domain $x = \lambda$.

The boundary conditions at the chimney wall $x = a(z, t)$ play a key role in describing the flow. Chimneys are narrow ($a \ll 1$) so they can be represented by singular interface conditions at $x = 0$. Lubrication theory applied to the flow in the narrow chimney yields the mass flux condition

$$\psi = \left[\frac{a^3}{3\mathrm{Da}(1 - \phi)^3} + a\right]\frac{\partial\psi}{\partial x} + \frac{3}{20}\frac{R_m}{\mathrm{Da}}a^3(\theta + 1), \tag{3}$$

where the prefactor for the forcing has been calculated from a quadratic Polhausen approximation [9,10]. Balancing the heat flux conducted into the chimney with that advected along the chimney yields $\theta_x = \psi\theta_z$. The chimney wall is a free boundary with net outflow and radius $a(z, t)$ determined from the condition [12]

$$\frac{\partial\theta}{\partial t} - \frac{\partial\theta}{\partial z} + \mathbf{u} \cdot \nabla\theta = 0. \tag{4}$$

The system, including conditions (2)–(4), was solved numerically by using second-order finite differences, with heat and concentration equations solved by semi-implicit Crank-Nicolson time stepping. Multigrid iteration was used to solve elliptic equations for ψ and θ [13,14]. Finally, $a(z, t)$ and $h(x, t)$ were treated as free boundaries and updated by using relaxation, the former being updated at each grid point to reduce the error in (4). The boundary layer approximation (2) leads to an unstable scheme for $h(x, t)$, so we use a one-parameter shape

$$h = h_1 - \psi_c[1 - \cosh\mu(\lambda - x)]/(\mu\sinh\mu\lambda), \tag{5}$$

where ψ_c is the stream function value at $\mathbf{x} = (0, h)$ (e.g., [9]). To remove a temperature singularity at the chimney top, this shape has a thermal boundary layer of width $1/\mu = R_m^{-2/3}$. The parameter h_1 is used to minimize the least-squares residual in (2), with $\theta = 0$ enforced at $z = h$. Importantly, the time-dependent initial value problem was integrated to a steady state, for imposed values of the chimney half-spacing $\lambda = lV/2\kappa$. The initial conditions were given either by a similarity solution with no fluid flow [8] or by continuation from a previous steady-state solution with different parameters. An arclength continuation scheme was also used to provide confirmation of the steady-state solution branches [15].

Using solutions for a range of λ and R_m with $\mathcal{C}$, $\mathcal{S}$, θ_∞, and Da held fixed, we study how chimney spacing and convective strength affects mushy layer dynamics. First we vary the chimney spacing wavelength λ with the Rayleigh number fixed at $R_m = 40$, noting that qualitatively similar behavior is observed for other values $27 \lesssim R_m \leq 60$.

The solute flux F_S from the mushy layer is shown as a function of chimney spacing λ in Fig. 2(a). There are two steady-state branches: a lower branch corresponding to a state of no flow and an upper branch describing convection with chimneys. Depending on the choice of initial conditions, hysteresis is found with one of two stable steady solutions over a range $\lambda_s < \lambda < \lambda_u$. A state of no flow remains stable for $\lambda < \lambda_u$ but becomes unstable for $\lambda > \lambda_u$ with the solution evolving in time to the upper branch of chimney convection. If we start on the upper branch and reduce λ, then chimney convection remains stable for $\lambda > \lambda_s$, but when $\lambda < \lambda_s$, chimneys collapse, returning the system to a state of no flow. Figure 2(b) traces the stability boundaries λ_s and λ_u versus R_m and identifies regions of phase space with no flow (I), chimney convection (II), and both steady states (III). Hence, starting in a state of chimney convection in region III and reducing λ, the system crosses the stability boundary $\lambda_s(R_m)$, the flow is stabilized, and chimney convection ceases. For $R_m \lesssim 27$, the stability curves cross so the nature of the solution changes. Calculations then indicate a state of weak convection with no chimneys, and $F_S = 0$ observed in region IV, where both chimney convection and no flow states are unstable.

Because there are always sufficiently large wavelengths λ available to trigger the instability of a state of no flow, we examine the upper solution branch to find that $F_S(\lambda)$ has a maximum at some critical wavelength $\lambda = \lambda_\mathcal{O}$. Hence, an optimal solute flux can be attained by varying the chimney spacing [Fig. 2(a)]. The solute flux weakens at large wavelengths $\lambda > \lambda_\mathcal{O}$, as seen by studying mushy layer properties at different chimney spacings. Figures 3(a) and 3(b) show profiles of steady-state θ, ϕ, and streamlines of Darcy velocity for $\lambda = 1.0$ at $\lambda > \lambda_\mathcal{O}$. At this large wavelength, approximately half of the mushy region is well drained by streamlines entering at the upper boundary and exiting through the chimney at $x = 0$. However, there is a large nearly stagnant region away from the chimney, explaining the observed inefficient drainage for large chimney spacings. Compare this to the corresponding profiles for the optimal configuration at $\lambda = \lambda_\mathcal{O}$ [Figs. 3(c) and 3(d)] where the streamlines show efficient drainage via convective cells of the order of one aspect ratio. Thus, rather than the drainage rate being controlled by buoyancy-driven flow in the chimney, the optimal solute flux is controlled by the efficiency of convection *within* the mushy region. For both wavelengths, θ and ϕ have qualitatively similar structure with significant horizontal variation of ϕ leading to inhomogeneity in the final material.

Having determined the system properties for a range of λ, we use the variational principle to select a preferred value of chimney spacing with maximal solute flux at $\lambda = \lambda_\mathcal{O}$ and calculate changes with R_m. For $R_m \gg 1$ we find that the optimal solute flux $F_{S\mathcal{O}}$ increases approximately linearly with R_m, giving the approximate scaling laws

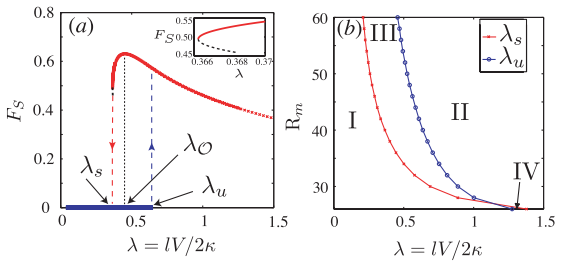

FIG. 2 (color online). (a) Steady-state solute fluxes $F_S(\lambda)$ exiting a mushy layer vary with the chimney spacing λ. Two branches of solutions are determined and exhibit hysteresis; the upper branch results from convection with chimneys (red crosses with $\lambda > \lambda_s$), and the lower branch results from a state of no flow and hence $F_S(\lambda) = 0$ (blue squares) which is unstable for $\lambda > \lambda_u$. Red and blue dashed lines indicate the trajectories at λ_s and λ_u, respectively. A maximal solute flux $F_{S\mathcal{O}}$ is attained for a chimney spacing $\lambda = \lambda_\mathcal{O}$, with weaker solute drainage at $\lambda > \lambda_\mathcal{O}$. The inset shows the upper stable branch (red curve) and intermediate unstable branch (black dashed curve) in the vicinity of the stabilization point confirmed by arclength continuation. Here $R_m = 40$, $\mathcal{C} = 15$, $\mathcal{S} = 5$, $\theta_\infty = 0.4$, and $\mathrm{Da} = 5 \times 10^{-3}$ for consistency with previous studies [10] which use properties for aqueous NH_4Cl. The optimal solute flux is approximated by (6) and (7), with $\gamma = 0.03$ and $R_c = 20$. (b) Stability curves tracing the variation of λ_s (red points) and λ_u (blue points) with R_m; all other parameters fixed. In I only the lower branch is stable, yielding no flow. In II only the upper branch is stable, yielding convection with chimneys. Hysteresis is observed with two steady states in III. Both no flow and chimney convection states are unstable in IV, yielding weak convection with no chimney.

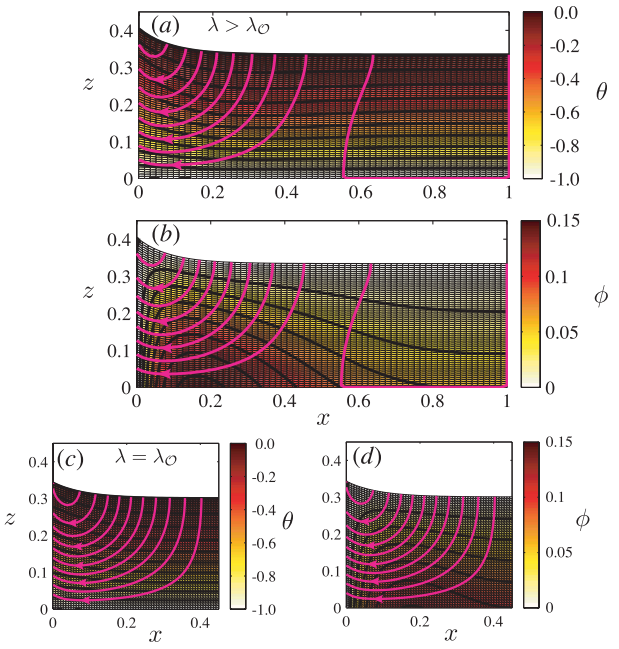

FIG. 3 (color online). Comparison of mushy region profiles at a long-wavelength chimney spacing $\lambda = 1.0 > \lambda_\mathcal{O}$ (a),(b) with those at the optimal spacing $\lambda = \lambda_\mathcal{O} = 0.46$ (c),(d). Here θ is shown by the color scale in (a),(c) with isotherms shown as solid black curves; ϕ is shown by the color scale in (b),(d), with constant ϕ contours as black curves, and Darcy velocity streamlines as magenta curves. Other parameters are as in Fig. 2.

$$F_S = 0, \qquad R_m < R_c, \tag{6}$$

$$F_S \sim \gamma(R_m - R_c), \qquad R_m \geq R_c, \tag{7}$$

for some constants γ and R_c that depend on the other parameters imposed on the system. For $R_m \gg 1$, Eq. (7) implies that the dimensional solute flux

$$\hat{F}_S \sim \gamma \rho_0 g \beta (C_0 - C_E)^2 \Pi_0 / \mu, \qquad R_m \gg 1, \tag{8}$$

is independent of both the thermal diffusivity κ and the solidification rate V. This is consistent with the rate of solute transport being controlled by the large scale convective flow, independent of any effective transport induced by molecular diffusion. As a point of comparison, the heat flux in turbulent Rayleigh-Bénard convection is also predicted to be asymptotically independent of κ in Kraichnan's ultimate strongly convective regime [16].

The optimal chimney spacing $\lambda_\mathcal{O}$ and resulting mushy layer depth $h_\mathcal{O}$ both decrease as the Rayleigh number increases, but the aspect ratio $\lambda_\mathcal{O}/h_\mathcal{O}$ asymptotes to a constant value for $R_m \gg 1$. The stronger flow at larger R_m generates a thinner mushy layer, but the most efficient solute drainage is given by order-one aspect ratio convective cells. This behavior is consistent with the constant mean aspect ratio observed in the transient phase of enthalpy method simulations [17].

These results suggest explanations for phenomena observed during transient growth, such as growth from a fixed temperature boundary. Experiments show that, as the mushy layer thickens over time, extinction of convective flow in some of the chimneys leads to an increase in their mean spacing [5]. This is consistent with (a) the dynamics of optimal chimney spacing which has constant aspect ratio $\lambda_\mathcal{O}/h_\mathcal{O}$ for $R_m \gg 1$ and (b) the mean spacing of chimneys increasing with mushy layer depth during transient growth. Also, during transient growth, the extinction of flow in certain chimneys can be interpreted via the flow stabilization found here for $\lambda \ll h$. Because the mean depth h increases with fixed chimney spacing λ during transient growth, the aspect ratio λ/h decreases until it stabilizes convection and extinguishes flow in a selection of the chimneys. In sum, this offers a possible explanation for the observed mechanisms of chimney coarsening as h increases. Comparison with previous work [5,18] suggests that the scaling (7) may also be relevant for transient growth at small concentration ratios ($\mathcal{C} \ll 1$). In particular, in experiments in a finite geometry [5], the solute flux (8) predicts that the concentration of the liquid region will change approximately linearly in time. This provides a simple parameterization of brine drainage from growing sea ice for large scale models without having to resolve natural horizontal variations in sea ice structure.

In summary, we have numerically analyzed strongly nonlinear convection in a solidifying mushy layer with a periodic array of chimneys with spacing λ. By varying λ, we have shown the existence of an optimal chimney spacing $\lambda_\mathcal{O}$ that maximizes the solute flux from the mushy layer and hence also the rate of removal of its potential energy. This $\lambda_\mathcal{O}$ yields convective cells of the order of one aspect ratio, thereby efficiently draining the mushy layer, with weak flow for $\lambda \gg \lambda_\mathcal{O}$. For $\lambda \ll \lambda_\mathcal{O}$ there is stabilization, so that chimney convection cannot be supported for spacings smaller than a Rayleigh-number-dependent critical value, which suggests a method to suppress chimney formation in engineering applications. Steady states of chimney convection and no flow show hysteretic behavior. These mechanisms are consistent with dynamics in this dissipative system controlled by a variational principle, with chimney spacing adjusting to optimize the rate of release of potential energy from the mushy layer, and facilitate the most efficient route towards thermodynamic equilibrium.

We thank the U.S. National Science Foundation Grant No. OPP0440841 and Yale University. We thank C. Doering for discussions at the beginning of this project.

[1] G. J. Sussman and J. Wisdom, *Structure and Interpretation of Classical Mechanics* (MIT Press, Boston, MA, 2001).
[2] C. R. Doering and P. Constantin, Phys. Rev. Lett. **69**, 1648 (1992).
[3] C. R. Doering, F. Otto, and M. G. Reznikoff, J. Fluid Mech. **560**, 229 (2006).
[4] M. G. Worster, in *Perspectives in Fluid Dynamics: A Collective Introduction to Current Research* (Cambridge University Press, Cambridge, England, 2000), pp. 393–446.
[5] J. S. Wettlaufer, M. G. Worster, and H. E. Huppert, J. Fluid Mech. **344**, 291 (1997).
[6] S. S. L. Peppin, H. E. Huppert, and M. G. Worster, J. Fluid Mech. **599**, 465 (2008).
[7] T. H. Solomon and R. R. Hartley, J. Fluid Mech. **358**, 87 (1998).
[8] M. G. Worster, J. Fluid Mech. **224**, 335 (1991).
[9] T. P. Schulze and M. G. Worster, J. Fluid Mech. **356**, 199 (1998).
[10] C. A. Chung and M. G. Worster, J. Fluid Mech. **455**, 387 (2002).
[11] P. W. Emms and A. C. Fowler, J. Fluid Mech. **262**, 111 (1994).
[12] T. P. Schulze and M. G. Worster, J. Fluid Mech. **541**, 193 (2005).
[13] W. L. Briggs, V. E. Henson, and S. F. McCormick, *A Multigrid Tutorial* (SIAM, Philadelphia, 2000).
[14] J. C. Adams, Appl. Math. Comput. **34**, 113 (1989).
[15] H. B. Keller, in *Applications of Bifurcation Theory* (Academic, New York, 1977), pp. 359–384.
[16] R. H. Kraichnan, Phys. Fluids **5**, 1374 (1962).
[17] R. F. Katz and M. G. Worster, J. Comput. Phys. **227**, 9823 (2008).
[18] D. Notz and M. G. Worster, J. Geophys. Res. Oceans **114**, C05006 (2009).